Journal of Magnetism and Magnetic Materials 475 (2019) 544–549

Contents lists available at ScienceDirect

Journal of Magnetism and Magnetic Materials

journal homepage: www.elsevier.com/locate/jmmm

Research articles

Towards enhancing the magnetic properties by morphology control of $ATiO_3$ (A = Mn, Fe, Ni) multiferroic materials

R.A.P. Ribeiro[a], L.H.S. Lacerda[a], E. Longo[b], J. Andrés[c,*], S.R. de Lazaro[a]

[a] Department of Chemistry, State University of Ponta Grossa, Av. General Carlos Cavalcanti, 4748, 84030-900 Ponta Grossa, PR, Brazil
[b] CDMF-UFSCar, Universidade Federal de São Carlos, PO Box 676, 13565–905 São Carlos, SP, Brazil
[c] Department of Analytical and Physical Chemistry, University Jaume I, Castelló 12071, Spain

ARTICLE INFO

Keywords:
$ATiO_3$
DFT
Magnetism
Multiferroic
Morphology
Wulff's construction
Surface energy
Spin density

ABSTRACT

Magnetic materials are of great interest due to their widespread applications in various technologies. Precise control of different aspects of the morphology and magnetic properties is a key aspect in establishing their relationship with material shapes and sizes. In this work, the density functional theory (DFT) is applied to investigate the surface structure and magnetic properties of low-index (1 1 0), (1 0 1), (1 0 0), (0 0 1), (1 1 1), (0 1 2) surfaces of $ATiO_3$ (A = Mn, Fe, Ni) multiferroic materials. In particular, a theoretical approach, based on the Wulff construction and magnetization density (M) index, is applied to infer the relationship between the morphology and surface magnetism. The results indicate that the magnetic properties of $ATiO_3$ materials can be controlled by the presence of exposed surfaces. In particular, the (0 0 1) and (1 1 1) surfaces are found to be adequate to enhance the superficial magnetism. The underlying reasons behind such mechanism are discussed from the perspective of uncompensated spins and charge-transfer processes along the exposed surfaces. This investigation suggests that the morphology-oriented $ATiO_3$ materials are good candidates for superior multiferroic applications.

1. Introduction

Theoretical and experimental studies involving magnetic materials combine a broad range of synthetic methods, and characterization techniques applying physics, chemistry, and materials science. The functionality of materials is strongly related to their structure, size, and shape. In this context, the unusual phenomena are associated to the emergence of quantum effects. In particular, the magnetic properties are very sensitive to the morphology due to the dominating role of anisotropy in magnetism when one or more dimensions are reduced [1–4].

The appearance of exposed surface and interface plays a fundamental role in the control of material properties. In particular, this is a key factor that exhibits intriguing magnetic properties at reduced dimensions. The exposed surface presents reduction of metal coordination, creating some vacancies along the exposed surfaces. This reduces the hopping of electrons from site to site, increasing the Coulomb interactions between the electrons. This also enhances the tendency of appearance of superficial magnetism, mainly due to the presence of uncompensated spins originated from the confinement quantum effects [2,5–7].

In the last few years, the combination between the theoretical and experimental techniques has allowed the design of functional materials where the morphological modulation is considered to be a fundamental approach to control several degrees of freedom involved in different physical and chemical processes. Different applications, such as catalysis, gas sensing, energy conversion and storage, and magnetoresistance depend on the surface arrangement at the atomic level [8–11]. The magnetic properties are also affected by the chemical composition, shape, size, and the local details at the core and surface of the sample. These are also dependent on the interactions with the surrounding environment that enables the existence of superparamagnetism, giant magnetic resistance, and superior multiferroic properties [12–16].

Magnetic materials are promising candidates for use in of spintronic technology, where both the electrical and magnetic degrees of freedom are used [2,4].Numerous experimental investigations have discussed the dependence of the surface morphology and unusual magnetic properties for different materials, such as Co_3O_4, Mn_xO_y, Fe_xO_y, $CoFe_2O_4$, and MnS [9,17–31].

Our recent efforts are devoted to developing an innovative and alternative method to relate the magnetic properties with crystal morphology using open-shell density functional theory (DFT), and Wulff

* Corresponding author.
E-mail address: andres@qfa.uji.es (J. Andrés).

https://doi.org/10.1016/j.jmmm.2018.12.002
Received 31 July 2018; Received in revised form 7 November 2018; Accepted 1 December 2018
Available online 01 December 2018
0304-8853/

construction. Under this approach, the magnetization density index (M) is evaluated by means of the uncompensated spins along the exposed surfaces, enabling the modulation of crystal morphology to obtain superior magnetic properties as observed for Co_3O_4 and $MnTiO_3$ [32,33].

In this study, we present a theoretical investigation to control the magnetic properties of $ATiO_3$ (A = Mn, Fe, Ni) multiferroic materials depending on the morphology, focusing on the description of uncompensated spins, surface exposed undercoordinated cations, and shape-oriented superficial magnetism.

2. Theoretical method and computational procedure

In this work, we calculate the surface energy (E_{surf}) by means of DFT calculations using hybrid PBE0 functional and CRYSTAL14 code [34,35]. The geometry of the (1 0 0), (0 0 1), (1 1 0), (1 0 1), (0 1 2), (1 1 1) surfaces are described using the slab construction with a thickness large enough to ensure full relaxation of the surface atoms and convergence of the surface energy. After completing the corresponding optimization process and thickness convergence test, the repeat units {number of layers in the slab} are selected as follows: for TiO_3A\{18 layers} and (0 0 1) surface, $O_3A_2Ti_2O_3$ {40 layers} for (1 1 0) surface, OTiOAO {30 layers} for (1 0 1) surface, $O_2A_2O_2Ti_2O_2$ {30 layers} for (0 1 2) surface, $O_2A_2Ti_2O_4$ {40 layers} for (1 0 0) surface, and $OTiOAOTiO_2AO$ {50 layers} for (1 1 1) surface. These layers were found to be sufficient for the convergence. In the course of the geometrical optimization, we do not place any constraints on the atoms except for the conservation of the original crystal symmetry in the two dimensions parallel to the surface.

It is important to note that (0 0 1), (1 0 0), (1 0 1), (0 1 2) and (1 1 1) surfaces are polar; therefore, the slab models used are differently terminated, while (1 1 0) is non-polar. Although different surface terminations may occur, only those giving rise to a minimal dipole moment are considered, as presented in Fig. 1.

In our study the surface energy (E_{surf}) is assumed to be the relaxed surface cleavage energy (E_{cleav}). Firstly, we introduce the concept of unrelaxed E_{cleav} as the required energy to cut the bulk along the selected plane.

$$E_{cleav}^{unrlx} = \frac{(E_{slab}^{unrlx} - nE_{bulk})}{2A}$$

Here, E_{slab}^{unrlx} and E_{bulk} correspond to the total energies for the unrelaxed slab model and the bulk unit, respectively, whereas n and A represent the number of bulk units used in the slab construction and the surface area, respectively. For polar surfaces, a relaxation process of both Z^+ and Z^- terminations is performed; then the $E_{relax}(Z^+|\ Z^-)$ is calculated as the difference between the total energies for relaxed and unrelaxed slabs, as follows:

$$E_{relax}(Z^+|\ Z^-) = \frac{(E_{slab}^{unrlx} - E_{slab}^{relax})}{2A}$$

being the E_{surf} the mean value for both terminations:

$$E_{surf} = E_{cleav}^{relax}(Z^+|\ Z^-) = E_{cleav}^{unrlx} - E_{relax}$$

In all calculations, A, Ti, and O centers were described from all-electron atomic basis sets composed of Gaussian type functions denominated by 86-411d41G, 86-51(3d)G, and 8-411, respectively [36–38]. It is important to recognize that the electron correlation effects are important in manganite materials. However, we are confident in our results because the computed bulk structural properties and band gaps for $ATiO_3$ are in agreement with the experimental results [39]. The diagonalization of the Fock matrix was performed at adequate k-point grids (Pack-Monkhorst) in the reciprocal space [40]. The thresholds controlling the accuracy of the Coulomb and Exchange integral calculations were controlled by five thresholds set to 7, 7, 7, 7, and 14; respectively. The irreducible Brillouin zone (IBZ) was represented by a number of sampling points, which were chosen as (8 × 8 × 8) and (4 × 4) for the bulk and the slab, respectively. As a result, there are 65 k-points in the bulk IBZ, and 4 k-points in the slab IBZ. The convergence criteria for mono- and bielectronic integrals were set to 10^{-8}Hartree. The RMS gradient, RMS displacement, maximum gradient, and maximum displacement were set to 3×10^{-5}, 1.2×10^{-4}, 4.5×10^{-5}, and 1.8×10^{-4} a.u., respectively.

The classical Wulff construction is employed where the energy of the crystal surface (E_{surf}) determines the equilibrium morphology. A simple relationship between (E_{surf}) and the distance in the normal direction from the center of the crystallite allows to find the ideal morphology. By tuning the surface energies of the different facets, the available morphologies can then be obtained [11,41–49].

The magnetic properties associated with the different morphologies were calculated using the spin density (D_μ) index of a given surface. This is related to the magnetic moment (μ_B) per unit cell area (A). In addition, the combination of the polyhedral representation, $c_{(hkl)}$, derived from the Wulff construction (with D_μ) enables us to predict the total magnetization density (M) index of a given morphology as follows [32]:

$$D_\mu = \frac{\mu_B}{A}$$

$$M = \sum c_{(hkl)} \bullet D_\mu^{(hkl)}$$

To link the obtained morphologies with the ideal shapes, the polyhedron energy (E_{pol}) was calculated by summing the contribution of each surface to morphology ($c_{[hkl]}$) and its E_{surf}, as follows:

$$E_{pol} = \sum c_{(hkl)} \bullet E_{surf}^{(hkl)}$$

where, $c_{(hkl)}$ is the "weight" or percentage contribution of the surface area to the total surface area of the polyhedron, and $E_{surf}^{(hkl)}$ is the surface energy of the corresponding surface. This methodology provides a simple relationship between the different morphologies, enabling an atomic level understanding of thermodynamic process involved in morphological modulations [48,50].

3. Results and discussion

3.1. $MnTiO_3$

In Table 1 the calculated E_{surf} values for $MnTiO_3$ are summarized. The resultant magnetic moment along the exposed surface and D_μ is also shown. In this case, it was observed that the stability order is (1 1 0) > (0 1 2) > (1 0 1) > (1 0 0) > (0 0 1) > (1 1 1), while the calculated magnetic moment along the different surfaces showed an unusual spin population compared to the bulk value. In particular, the polar (0 0 1) and (1 1 1) surfaces showed the highest values of D_μ. This is in agreement with the undercoordinated species exposed in such surfaces. In our previous work, the superficial magnetism was increased from the charge transfer mechanism between the neighboring clusters. This followed the Kroger-Vink notation, where a charge accumulation on superficial [TiO_n]' clusters for (0 0 1) and (1 1 1) surfaces was found using the equation below:

$$[MnO_n]^x + [TiO_n]^x \rightarrow [TiO_n]' + [MnO_{n-1}...V_O^{\cdot}]$$

Wulff construction were developed using the calculated E_{surf} values (Table 1)to conduct the morphological modulation of $MnTiO_3$with a view to attaining superior magnetic properties. The obtained shapes with highest values of M are shown in Fig. 2. The vacuum ideal morphology proposed by $MnTiO_3$ exhibited a corner-truncated cylindrical shape that predominantly exposed the (1 1 0) surface, and to a minor extent, the (0 1 2) and (0 0 1) surfaces. Despite the higher value of E_{surf} for (0 0 1) surface, the ideal morphology of $MnTiO_3$ showed an extent of this surface, suggesting the existence of an intriguing magnetic behavior due to the exposure of unusual magnetic Ti species. Indeed, the

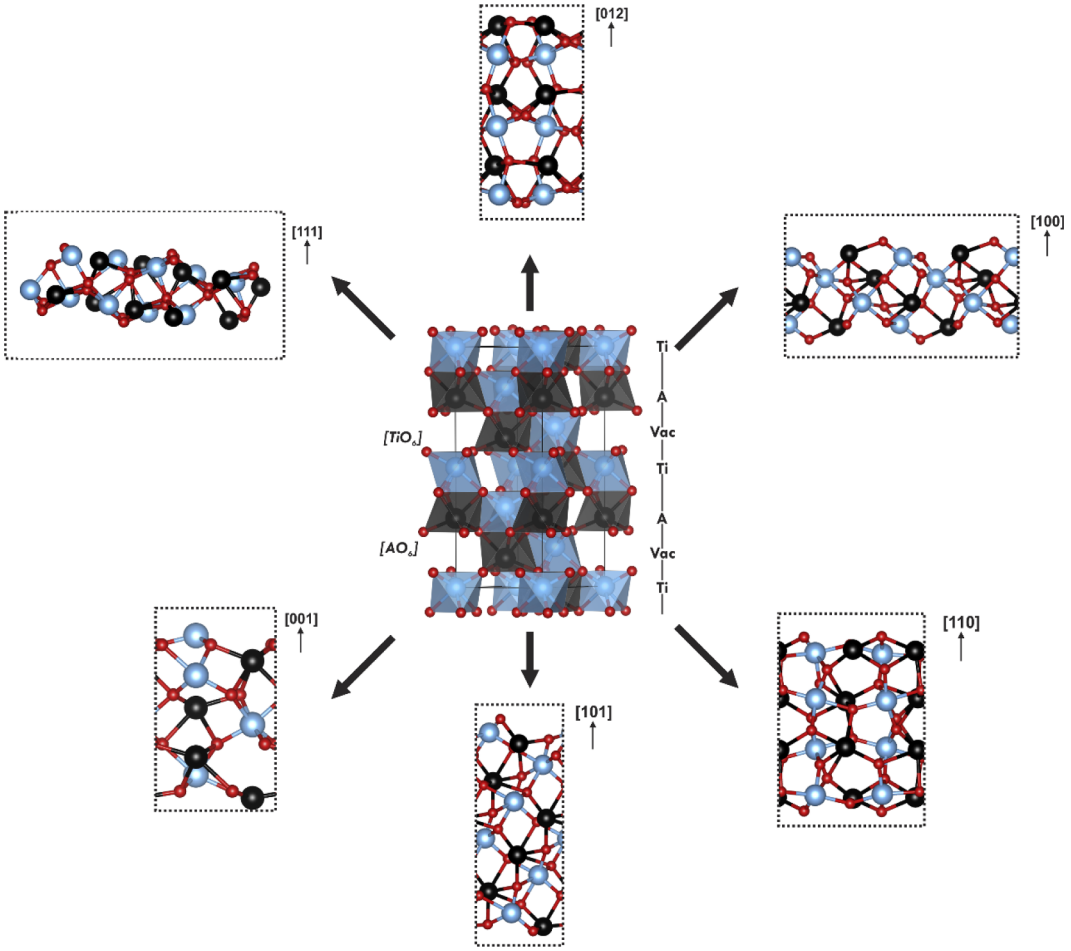

Fig. 1. Crystalline unit cell of $ATiO_3$ (A = Mn, Fe, Ni) materials and its surface slabs. The black, blue, and red balls represent A (Mn, Fe, Ni), Ti, and O ions, respectively. The dashed lines represent the lattice vector used in the calculations. (For interpretation of the references to color in this figure legend, the reader is referred to the web version of this article.)

Table 1
Surface energy (E_{surf}), area (A), magnetic moment and magnetization density (D_μ) calculated for the $MnTiO_3$ surfaces.

Surfaces	Esurf (J m^{-2})	A (nm^2)	Magnetic Moment (μb)			Dμ (μb nm^{-2})
			Z^+	Z^-	Total	
(1 0 0)	2.07	0.710	0	0	0	0
(0 0 1)	2.64	0.235	−0.50	−4.40	−4.90	20.87
(1 1 0)	0.70	0.410	0	0	0	0
(1 0 1)	2.02	0.249	4.70	−4.70	0	0
(0 1 2)	1.98	0.284	−0.20	0	−0.20	0.71
(1 1 1)	3.46	1.252	0.50	0.30	0.80	0.64

increased superficial magnetism for $MnTiO_3$ morphology can be modulated by tuning the E_{surf} values for (0 0 1) and (1 1 1) surfaces.

In the reaction path (A) of Fig. 2 a polyhedral that exposes mainly (1 1 1) surface(with a few extent of both (0 1 2) and (0 0 1) surfaces) was obtained controlling the ratio between E_{surf} values for both (1 1 0) and (1 1 1) surfaces. In this path, a superior M value (M = 6.51) was found, which is attributed to the exposure of both (0 0 1) and (1 1 1) surfaces that exhibit an increased magnetic moment (Table 1).

On the other hand, in the path (B) of the Fig. 2, the cylindrical shape (containing only (1 1 0) and (0 0 1) exposed surfaces) was obtained controlling the ratio between the E_{surf} values. This resulted in an increased superficial magnetism (M = 6.48) due to the superior contribution of (0 0 1) surface in comparison to the ideal morphology (M = 5.53). Recently, Wang *et al*[51]obtained $MnTiO_3$nanodiscs that preferentially exposed (0 0 1) surfaces with a few extent of (1 1 0), which can be compared with the theoretical prediction of nanodisc morphology by controlling the E_{surf} ratio for these surfaces, resulting in superior magnetic properties (M = 12.76), which are in agreement with the experimental results [51].

In short, our results suggest that in case of multiferroic shape-oriented $MnTiO_3$, superior multiferroic properties can be obtained by controlling the exposure of (0 0 1) and (1 1 1) surfaces due to the presence of reduced $[TiO_n]$' clusters.

3.2. $FeTiO_3$

Here the E_{surf} values of $FeTiO_3$are calculated, and the spin densities along the surfaces are investigated, as presented in Table 2.

A different stability order was observed in comparison to $MnTiO_3$. Here, the thermodynamic stability order of the surfaces was: (1 1 0) > (0 1 2) > (1 0 0) > (0 0 1) > (1 0 1) > (1 1 1). This shows a change between (1 0 0), (0 0 1) and (1 0 1) surfaces in comparison to $MnTiO_3$. This fact can be attributed to the chemical bond anisotropy along the surface–once the covalent character is distinguished along the Fe-O and Mn-O bonds. In addition, we noted an increase in the E_{surf} value for non-polar (1 1 0) surface in comparison to $MnTiO_3$. This is associated with the increased covalent character of the Fe-O bonds resulting in a higher required energy to create slab model cutting for this surface. In addition, our results suggest a singular spin population for the polar (0 0 1) and (1 1 1) surfaces, resulting from the charge transfer between $[AO_n]$ and $[TiO_n]$ (n = 2–5) clusters in order to generate

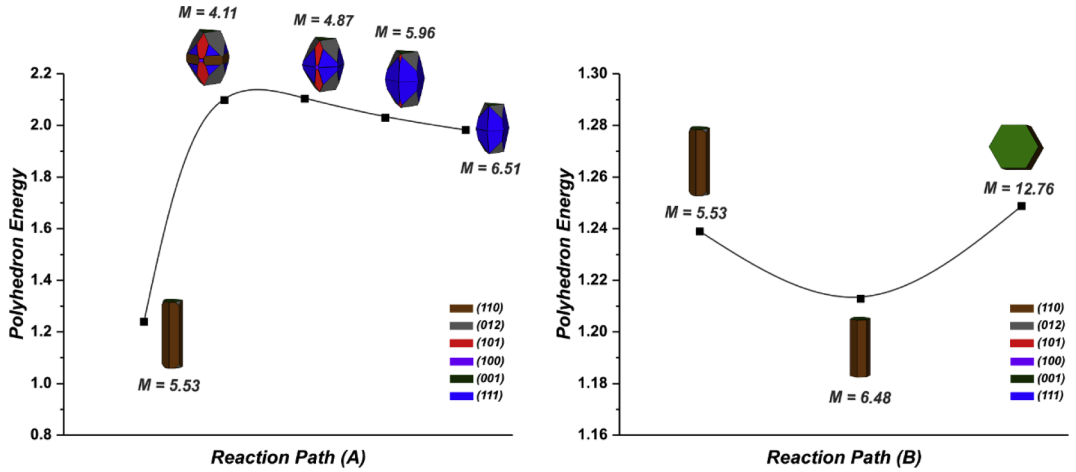

Fig. 2. Schematic representation of the energy profile to obtain different $MnTiO_3$ morphologies. The intermediate morphologies are obtained by decreasing/increasing the E_{surf} values of the corresponding surfaces involved in the process.

Table 2
Surface energy (E_{surf}), area (A), magnetic moment and magnetization density (D_μ) calculated for the $FeTiO_3$ surfaces.

Surfaces	E_{surf}(J m^{-2})	A (nm^2)	Magnetic Moment (μ_b)			D_μ (μ_b nm^{-2})
			Z^+	Z^-	Total	
(1 0 0)	2.00	0.702	0	0	0	0
(0 0 1)	2.23	0.230	−0.74	−3.71	−4.45	19.33
(1 1 0)	1.57	0.405	0	0	0	0
(1 0 1)	2.25	0.246	3.89	−3.89	0	0
(0 1 2)	1.85	0.280	0	0	0	0
(1 1 1)	3.89	1.237	−0.73	−0.32	−1.04	0.84

reduced [TiO_n]' clusters, as discussed previously.

As for $MnTiO_3$, the morphological map of $FeTiO_3$ was investigated considering the E_{surf} values and the spin density along the surface, aiming to select and predict the morphologies with superior magnetic and multiferroic properties, as presented in Fig. 3.

The vacuum ideal morphology of $FeTiO_3$ was mainly composed by (1 1 0) and (0 1 2) surfaces with a minor extent of (0 0 1) and (1 0 1), corresponding to a corner and edge-truncated cylindrical shape. The exposure of (0 0 1) surface induces a M = 4.99, suggesting that the control of superficial magnetism for $FeTiO_3$ can be made by controlling the ratio between E_{surf} values for (0 0 1) and (1 1 1), due to the increased spin density along the surfaces. Indeed, in the path (A) of Fig. 3, the control of E_{surf} for (1 1 1) generates different shapes with increased contribution of this surface, resulting in increased superficial magnetism even compared with $MnTiO_3$. In this path, the thermodynamic pathway to obtain superior magnetic properties requires an activation energy associated with the increase of E_{surf} values for (1 1 0) and (0 1 2) surfaces summed to the stabilization of (1 1 1) surface.

On the other hand, in the reaction path (B) of Fig. 3 only the E_{surf} value for (0 0 1) was changed, generating distinct truncated cylindrical shapes with an increased contribution of (0 0 1) surface that exhibits singular magnetic properties along the surface. This results in an increased superficial magnetism moving from the ideal (M = 4.99) to the hexagonal cylindrical shape (M = 12.36). In comparison to the experimental results for hexagonal nanodisc of $MnTiO_3$ [51], the predicted shape for $FeTiO_3$ shows a higher value of unpaired electrons along the exposed surfaces, being an excellent candidate for multiferroic applications.

3.3. $NiTiO_3$

The calculated energy and magnetic properties of $NiTiO_3$ are presented in Table 3. For this material, the stability order of the surfaces, based on the E_{surf} values, was: (1 1 0) > (0 1 2) > (1 0 0) > (0 0 1) > (1 0 1) > (1 1 1). This shows the same order observed for $FeTiO_3$. This result can also be supported by the increase of the covalent character for both A-O and Ti-O moving from Mn to Ni in $ATiO_3$, as it was demonstrated by a QTAIM analysis carried out for bulk $ATiO_3$ (A = Mn, Fe, Ni)[39]. The two-dimensional slabs, formed by cutting the bulk along the selected surfaces, provoke a chemical anisotropy along the crystalline structure. Therefore, this increase the covalent character of both A-O bonds, moving from Mn to Ni, decreasing the electron mobility.

By analyzing the spin density distribution, it was observed that (0 0 1) and (1 1 1) surfaces show a singular spin density along the

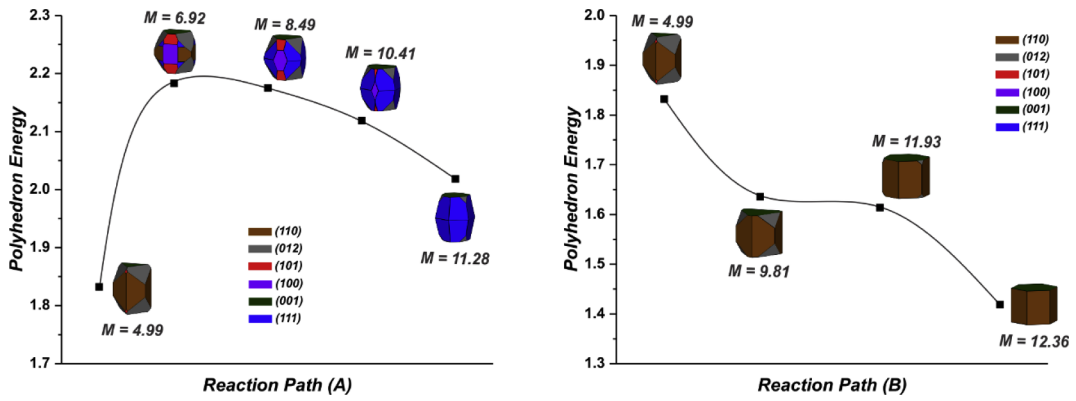

Fig. 3. Schematic representation of the energy profile to obtain different $FeTiO_3$ morphologies.

Table 3
Surface energy (E_{surf}), area (A), magnetic moment and magnetization density (D_μ) calculated for the $NiTiO_3$ surfaces.

Surfaces	E_{surf} (J m^{-2})	A (nm^2)	Magnetic Moment (μ_b)			D_μ (μ_b nm^{-2})
			Z^+	Z^-	Total	
(1 0 0)	2.43	0.691	0	0	0	0
(0 0 1)	2.46	0.220	0	−1.69	−1.69	7.70
(1 1 0)	1.92	0.399	0	0	0	0
(1 0 1)	2.78	0.242	1.68	−1.68	0	0
(0 1 2)	2.38	0.273	0	0	0	0
(1 1 1)	5.64	1.217	0.30	−0.59	−0.29	0.24

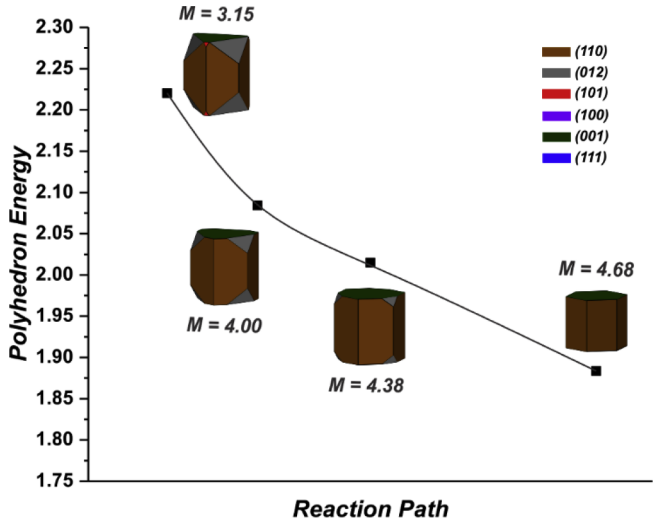

Fig. 4. Schematic representation of the energy profile to obtain different $NiTiO_3$ morphologies.

exposed surfaces related to the uncompensated spins. However, because of the increased covalent character associated with the Ni-O bonds, the creation of oxygen vacancies along the surface does not induce the charge transfer between [NiO_n] and [TiO_n] clusters (n = 2–5). This suggests a higher spin density redistribution in empty 3d orbitals of Ni^{2+}, reducing the magnetic moment along the surfaces. Due to the exposure of uncompensated Ni^{2+} spins, (0 0 1) is the best surface to induce superficial magnetism in $NiTiO_3$.

Considering the E_{surf} values of Table 3 and the Wulff construction, a corner and edge-truncated cylindrical ideal morphology is obtained (Fig. 4). As observed, (1 1 0) and (0 1 2) surfaces are the most stable surfaces, followed by (0 0 1) surface, and a minor extent of (1 0 1) surface. The superficial magnetism calculated for the ideal morphology shows the smallest value (M = 3.15) along the $ATiO_3$ (A = Mn, Fe, Ni) series, which is attributed to the lowest spin density along the exposed surfaces. To increase the superficial magnetism in $NiTiO_3$, the control of (0 0 1), (1 1 0) and (0 1 2) surfaces' E_{surf} values can be adjusted to induce a higher M for the hexagonal nanodisc (M = 4.68). This shows that such surface plays a fundamental role in the control of magnetic properties of $NiTiO_3$. This result confirms the experimental observations associated with the growth mechanism of $NiTiO_3$thin-films that expose (0 0 1) surfaces with increased weak ferromagnetism and superior multiferroic properties [52–54].

In this work, we have presented a systematic investigation about the morphological modulations of multiferroic $ATiO_3$ (A = Mn, Fe, Ni) using an alternative and innovative method that suggests that enhanced magnetic properties can be obtained by controlling the exposure of (0 0 1) and (1 1 1) surfaces for $MnTiO_3$ and $FeTiO_3$, respectively. On the contrary, for $NiTiO_3$ the (0 0 1) surface is mandatory.

These results combine an atomic-level description of the uncompensated spins along the exposed surfaces, charge transfer mechanism between the exposed clusters centered in under coordinated cations, as well as thermodynamic manipulation of E_{surf} values in order to select the morphologies with increased magnetization density index. The main novelty of our work is in suggesting the best morphologies for multiferroic applications. It was found that $ATiO_3$ (A = Mn, Fe, Ni) is an excellent candidate for this type of niche applications

Finally, it is important to note that the calculated morphologies are associated to the stabilization and/or destabilization of the exposed surfaces, and the magnetic properties are linked to the presence of excited electronic states. The combination of the structural and electronic disorder at the exposed surfaces introduces different kinds of dangling bonds that are capable of creating under coordinated cations along the exposed surfaces while cutting the bulk of $ATiO_3$ (A = Mn, Fe, Ni). Therefore, the excited electronic states concentrate near the fundamental electronic state with intriguing magnetic properties. This possibility and the mechanism behind the stabilization and characterization of the excited electronic states in this class of materials will be reported in forthcoming studies.

4. Conclusions

In this study, DFT calculations were performed to obtain the surface energies and the corresponding morphologies based on the Wulff construction and spin density. By considering the uncompensated spins of a given surface as well as the pathways between vacuum ideal morphology and a given shape, the magnetic properties of $ATiO_3$ (A = Mn, Fe, Ni) materials are analyzed. By controlling the ratio of the surface energy value, different kinds of morphologies were predicted. In case of $MnTiO_3$ and $FeTiO_3$, the results indicate that the control of (0 0 1) and (1 1 1) exposed surfaces lead to shape-oriented materials with increased superficial magnetism associated with the exposure of reduced [TiO_n]' species and uncompensated spins. On the other hand, for $NiTiO_3$, the control of (0 0 1) exposed surface is the best way to select the morphologies with highest superficial magnetism due to the chemical character associated with the Ni-O bonds. The ability to produce $ATiO_3$ (A = Mn, Fe, Ni) nanoparticles with high magnetization is highly desirable because of the remarkable multiferroic applications associated with such compounds. Based on these experimental results reported in the literature to date, we can conclude that by controlling the crystallinity and the exposed surface of the materials, it is possible to influence the magnetization properties of $ATiO_3$ (A = Mn, Fe, Ni) materials. Further investigations aiming at expanding the application of this approach to other materials with potential magnetic properties are currently in-progress in our laboratory.

Acknowledgments

This work was supported by the State University of Ponta Grossa, Universitat Jaume I, and CAPES and Araucaria Foundation. The authors acknowledge the financial support of the following agencies: Universitat Jaume I, for project UJI-B2016-25, Generalitat Valenciana for PrometeoII/2014/022, Prometeo/2016/079, ACOMP/2014/270, ACOMP/2015/1202, Ministerio de Economia y Competitividad, project CTQ2015-65207-P.

References

[1] D. Lisjak, A. Mertelj, Anisotropic magnetic nanoparticles: a review of their properties, syntheses and potential applications, Progr. Mater. Sci. 95 (2018) 286–328.
[2] R. Singh, Unexpected magnetism in nanomaterials, J. Magn. Magn. Mater. 346 (2013) 58–73.
[3] D.L. Leslie-Pelecky, R.D. Rieke, Magnetic properties of nanostructured materials, Chem. Mater. 8 (1996) 1770–1783.
[4] F.Y. Ping, S. Lei, Y. Ming, W. Aizhu, Z. Minggang, W. Qingyun, C. Sandhya, C. Ching-Ray, Prospects of spintronics based on 2D materials, Wiley

Interdisciplinary reviews: computational molecular, Science 7 (2017) e1313.
[5] Q.A. Pankhurst, R.J. Pollard, Origin of the spin-canting anomaly in small ferrimagnetic particles, Phys. Rev. Lett. 67 (1991) 248–250.
[6] J.I. Martín, J. Nogués, K. Liu, J.L. Vicent, I.K. Schuller, Ordered magnetic nanostructures: fabrication and properties, J. Magn. Magn. Mater. 256 (2003) 449–501.
[7] M. Springborg, M. Zhou, M. Molayem, B. Kirtman, Surfaces, shapes, and bulk properties of crystals, J. Phys. Chem. C 122 (2018) 11926–11932.
[8] A. Seyed-Razavi, I.K. Snook, A.S. Barnard, Origin of nanomorphology: does a complete theory of nanoparticle evolution exist? J. Mater. Chem. 20 (2010) 416–421.
[9] Y. Xia, X. Xia, H.-C. Peng, Shape-controlled synthesis of colloidal metal nanocrystals: thermodynamic versus kinetic products, J. Am. Chem. Soc. 137 (2015) 7947–7966.
[10] S.J.L. Billinge, I. Levin, The problem with determining atomic structure at the nanoscale, Science 316 (2007) 561–565.
[11] G.D. Barmparis, Z. Lodziana, N. Lopez, I.N. Remediakis, Nanoparticle shapes by using Wulff constructions and first-principles calculations, Beilstein J. Nanotechnol. 6 (2015) 361–368.
[12] H. Wu, L. Li, L.-Z. Liang, S. Liang, Y.-Y. Zhu, X.-H. Zhu, Recent progress on the structural characterizations of domain structures in ferroic and multiferroic perovskite oxides: a review, J. Eur. Ceram. Soc. 35 (2015) 411–441.
[13] B. Issa, I.M. Obaidat, B.A. Albiss, Y. Haik, Magnetic nanoparticles: surface effects and properties related to biomedicine applications, Int. J. Mol. Sci. 14 (2013) 21266–21305.
[14] M. Mikhaylova, D.K. Kim, N. Bobrysheva, M. Osmolowsky, V. Semenov, T. Tsakalakos, M. Muhammed, Superparamagnetism of magnetite nanoparticles: dependence on surface modification, Langmuir 20 (2004) 2472–2477.
[15] D.X. Chen, A. Sanchez, E. Taboada, A. Roig, N. Sun, H.C. Gu, Size determination of superparamagnetic nanoparticles from magnetization curve, J. Appl. Phys. 105 (2009) 083924.
[16] N.H. Hong, J. Sakai, N. Poirot, V. Brizé, Room-temperature ferromagnetism observed in undoped semiconducting and insulating oxide thin films, Phys. Rev. B 73 (2006) 132404.
[17] G. Anandha Babu, G. Ravi, Y. Hayakawa, M. Kumaresavanji, Synthesis and calcinations effects on size analysis of Co_3O_4 nanospheres and their superparamagnetic behaviors, J. Magn. Magn. Mater. 375 (2015) 184–193.
[18] P. Guo, G. Zhang, J. Yu, H. Li, X.S. Zhao, Controlled synthesis, magnetic and photocatalytic properties of hollow spheres and colloidal nanocrystal clusters of manganese ferrite, Colloids Surf., A 395 (2012) 168–174.
[19] D. Jagadeesan, U. Mansoori, P. Mandal, A. Sundaresan, M. Eswaramoorthy, Hollow spheres to nanocups: tuning the morphology and magnetic properties of single-crystalline α-Fe_2O_3 nanostructures, Angew. Chem. Int. Ed. 47 (2008) 7685–7688.
[20] Y.W. Jun, Y.Y. Jung, J. Cheon, Architectural control of magnetic semiconductor nanocrystals, J. Am. Chem. Soc. 124 (2002) 615–619.
[21] D. Liu, X. Wang, X. Wang, W. Tian, Y. Bando, D. Golberg, Co3O4 nanocages with highly exposed 110 facets for high-performance lithium, storage 3 (2013) 2543.
[22] J. Ma, J. Lian, X. Duan, X. Liu, W. Zheng, α-Fe_2O_3: Hydrothermal synthesis, magnetic and electrochemical properties, J. Phys. Chem. C 114 (2010) 10671–10676.
[23] D.T. Margulies, F.T. Parker, F.E. Spada, R.S. Goldman, J. Li, R. Sinclair, A.E. Berkowitz, Anomalous moment and anisotropy behavior in Fe_3O_4 films, Phys. Rev. B – Cond. Matter Mater. Phys. 53 (1996) 9175–9187.
[24] S. Mitra, S. Das, K. Mandal, S. Chaudhuri, Synthesis of a α-Fe_2O_3 nanocrystal in its different morphological attributes: growth mechanism, optical and magnetic properties, Nanotechnology 18 (2007).
[25] Q. Song, Z.J. Zhang, Shape control and associated magnetic properties of spinel cobalt ferrite nanocrystals, J. Am. Chem. Soc. 126 (2004) 6164–6168.
[26] D. Su, S. Dou, G. Wang, Single crystalline Co_3O_4 nanocrystals exposed with different crystal planes for Li-O_2 batteries, Sci. Rep. 4 (2014).
[27] A.S. Teja, P.-Y. Koh, Synthesis, properties, and applications of magnetic iron oxide nanoparticles, Prog. Cryst. Growth Charact. Mater. 55 (2009) 22–45.
[28] X. Wang, L. Yu, X.L. Wu, F. Yuan, Y.G. Guo, Y. Ma, J. Yao, Synthesis of single-crystalline Co_3O_4 octahedral cages with tunable surface aperture and their lithium storage properties, J. Phys. Chem. C 113 (2009) 15553–15558.
[29] J. Xiao, Q. Kuang, S. Yang, F. Xiao, S. Wang, L. Guo, Surface structure dependent electrocatalytic activity of Co_3O_4 anchored on graphene sheets toward oxygen reduction reaction, Sci. Rep. 3 (2013).
[30] X.L. Xu, Z.H. Chen, Y. Li, W.K. Chen, J.Q. Li, Bulk and surface properties of spinel Co_3O_4 by density functional calculations, Surf. Sci. 603 (2009) 653–658.
[31] J. Tuček, R. Zbořil, A. Namai, S.-I. Ohkoshi, ε-Fe_2O_3: an advanced nanomaterial exhibiting giant coercive field, millimeter-wave ferromagnetic resonance, and magnetoelectric coupling, Chem. Mater. 22 (2010) 6483–6505.
[32] R.A.P. Ribeiro, S.R. de Lazaro, L. Gracia, E. Longo, J. Andrés, Theoretical approach for determining the relation between the morphology and surface magnetism of Co_3O_4, J. Magn. Magn. Mater. 453 (2018) 262–267.
[33] R.A.P. Ribeiro, J. Andrés, E. Longo, S.R. Lazaro, Magnetism and multiferroic properties at MnTiO3 surfaces: A DFT study, Appl. Surf. Sci. 452 (2018) 463–472.
[34] C. Adamo, V. Barone, Toward reliable density functional methods without adjustable parameters: the PBE0 model, J. Chem. Phys. 110 (1999) 6158–6170.
[35] R. Dovesi, R. Orlando, A. Erba, C.M. Zicovich-Wilson, B. Civalleri, S. Casassa, L. Maschio, M. Ferrabone, M. De La Pierre, P. D'Arco, Y. Noël, M. Causà, M. Rérat, B. Kirtman, CRYSTAL14: a program for theab initioinvestigation of crystalline solids, Int. J. Quantum Chem. 114 (2014) 1287–1317.
[36] I. de P.R. Moreira, R. Dovesi, C. Roetti, V.R. Saunders, R. Orlando, Ab initio study of MF2 (M = Mn, Fe Co, Ni) rutile-type compounds using the periodic unrestricted Hartree-Fock approach, Phys. Rev. B 62 (2000) 7816–7823.
[37] F. Corà, The performance of hybrid density functionals in solid state chemistry: the case of $BaTiO_3$, Mol. Phys. 103 (2005) 2483–2496.
[38] M.D. Towler, N.L. Allan, N.M. Harrison, V.R. Saunders, W.C. Mackrodt, E. Aprà, Ab initio study of MnO and NiO, Phys. Rev. B 50 (1994) 5041–5054.
[39] R.A.P. Ribeiro, S.R. de Lazaro, C. Gatti, The role of exchange–correlation functional on the description of multiferroic properties using density functional theory: the $ATiO_3$ (A = Mn, Fe, Ni) case study, RSC Adv. 6 (2016) 101216–101225.
[40] H.J. Monkhorst, J.D. Pack, Special points for Brillouin-zone integrations, Phys. Rev. B 13 (1976) 5188–5192.
[41] T.L. Einstein 5 - Equilibrium Shape of Crystals A2 - Nishinaga, Tatau, in: Handbook of Crystal Growth (Second 2015 Edition), Elsevier Boston 215 264.
[42] M.M. Ferrer, A.F. Gouveia, L. Gracia, E. Longo, J. Andrés, A 3D platform for the morphology modulation of materials: first principles calculations on the thermodynamic stability and surface structure of metal oxides: Co_3O_4, α-Fe_2O_3, and In_2O_3, Modell. Simul. Mater. Sci. Eng. 24 (2016).
[43] The Wulff theorem R. Cerf J. Picard The Wulff Crystal in Ising and Percolation Models: Ecole d'Eté de Probabilités de Saint-Flour XXXIV – 2004 2006 Springer Berlin Heidelberg, Berlin, Heidelberg 189 199.
[44] P.F.S. Pereira, C.C. Santos, A.F. Gouveia, M.M. Ferrer, I.M. Pinatti, G. Botelho, J.R. Sambrano, I.L.V. Rosa, J. Andrés, E. Longo, α-$Ag_{2-2x}Zn_xWO_4$ ($0 \leq x \leq 0.25$) solid solutions: structure, morphology, and optical properties, Inorg. Chem. 56 (2017) 7360–7372.
[45] A.F. Gouveia, M.M. Ferrer, J.R. Sambrano, J. Andrés, E. Longo, Modeling the atomic-scale structure, stability, and morphological transformations in the tetragonal phase of $LaVO_4$, Chem. Phys. Lett. 660 (2016) 87–92.
[46] J. Andrés, L. Gracia, A.F. Gouveia, M.M. Ferrer, E. Longo, Effects of surface stability on the morphological transformation of metals and metal oxides as investigated by first-principles calculations, Nanotechnology 26 (2015) 405703.
[47] M.C. Oliveira, L. Gracia, M. de Assis, I.L.V. Rosa, M.F. do Carmo Gurgel, E. Longo, J. Andrés, Mechanism of photoluminescence in intrinsically disordered $CaZrO_3$ crystals: first principles modeling of the excited electronic states, J. Alloy. Compd. 722 (2017) 981–995.
[48] L.X. Lovisa, M.C. Oliveira, J. Andrés, L. Gracia, M.S. Li, E. Longo, R.L. Tranquilin, C.A. Paskocimas, M.R.D. Bomio, F.V. Motta, Structure, morphology and photoluminescence emissions of $ZnMoO_4$: $RE^{3+} = Tb^{3+}$ - Tm^{3+} - X Eu^{3+} (x = 1, 1.5, 2, 2.5 and 3 mol%) particles obtained by the sonochemical method, J. Alloys Compounds 750 (2018) 55–70.
[49] V.M. Longo, L. Gracia, D.G. Stroppa, L.S. Cavalcante, M. Orlandi, A.J. Ramirez, E.R. Leite, J. Andrés, A. Beltrán, J.A. Varela, E. Longo, A joint experimental and theoretical study on the nanomorphology of $CaWO_4$ crystals, J. Phys. Chem. C 115 (2011) 20113–20119.
[50] N.G. Macedo, A.F. Gouveia, R.A. Roca, M. Assis, L. Gracia, J. Andrés, E.R. Leite, E. Longo, Surfactant-mediated morphology and photocatalytic activity of α-Ag_2WO_4 material, J. Phys. Chem. C 122 (2018) 8667–8679.
[51] H. Wang, Q. Gao, H.T. Li, M. Gao, B. Han, K.S. Xia, C.-G. Zhou, Simple and controllable synthesis of high-quality $MnTiO_3$ nanodiscs and their application as a highly efficient catalyst for H_2O_2-mediated oxidative degradation, ACS Appl. Nano Mater. 1 (2018) 2727–2738.
[52] T. Varga, T.C. Droubay, M.E. Bowden, L. Kovarik, D. Hu, S.A. Chambers, Strain-dependence of the structure and ferroic properties of epitaxial $NiTiO_3$ thin films grown on different substrates, Adv. Condens. Matter Phys. 2015 (2015) 9.
[53] T. Varga, T.C. Droubay, L. Kovarik, M.I. Nandasiri, V. Shutthanandan, D. Hu, B. Kim, S. Jeon, S. Hong, Y. Li, S.A. Chambers, Coupled lattice polarization and ferromagnetism in multiferroic $NiTiO_3$ thin films, ACS Appl. Mater. Interfaces 9 (2017) 21879–21890.
[54] T. Varga, T.C. Droubay, M.E. Bowden, R.J. Colby, S. Manandhar, V. Shutthanandan, D. Hu, B.C. Kabius, E. Apra, W.A. Shelton, S.A. Chambers, Coexistence of weak ferromagnetism and polar lattice distortion in epitaxial $NiTiO_3$ thin films of the $LiNbO_3$-type structure, J. Vac. Sci. Technol. B 31 (2013) 030603.